



15th Canadian Masonry Symposium
Ottawa, Canada
June 2-5, 2025



**Experimental Testing of Controlled Rocking Masonry Walls
Incorporating Rubber Pads for Enhanced Seismic Performance**

Yara Solimanⁱ, Mohamed Ezzeldinⁱⁱ, and Lydell Wiebeⁱⁱⁱ

ABSTRACT

Most controlled rocking masonry walls (CRMWs) that have been studied previously depend on unbonded post-tensioning (PT) tendons for self-centering but often suffer from high prestressing losses and challenging repairs after damage. The current study examines an innovative CRMW design that eliminates unbonded PT tendons, instead relying on vertical gravity loads for self-centering. By integrating rubber pads to mitigate toe crushing, this new design not only minimizes structural damage but also significantly enhances lateral displacement capacity, offering a more resilient and efficient alternative to conventional masonry systems. The test wall, constructed from half-scale fully-grouted concrete masonry blocks and equipped with steel flexural yielding arms as externally-mounted energy dissipation devices, was subjected to dynamic snap-back testing and quasi-static cyclic loading. The experimental results are presented, including free vibration response, equivalent viscous damping, and force-displacement characteristics. The findings highlight the system's effectiveness in reducing damage and enhancing lateral displacement capacity compared to conventional masonry systems. The results also highlight the potential of rubber pads in mitigating compression toe issues and further improving the seismic resilience of CRMWs.

KEYWORDS

self-centering, controlled rocking, experimental testing, dynamic, rubber pads, reinforced masonry walls

ⁱ Ph.D. Candidate, McMaster University, Hamilton, Canada, solimy1@mcmaster.ca

ⁱⁱ Associate Professor, McMaster University, Hamilton, Canada, ezzeldms@mcmaster.ca

ⁱⁱⁱ Professor, McMaster University, Hamilton, Canada, wiebel@mcmaster.ca



INTRODUCTION

The design of earthquake-resistant structures follows the capacity design philosophy, which ensures that specific structural components, such as plastic hinges in reinforced masonry walls, yield during seismic events. This controlled yielding dissipates seismic energy while preserving the structure's integrity and prioritizing the occupants' safety. However, this approach frequently results in significant structural damage and residual drifts, complicating post-earthquake repair efforts. For instance, when residual drifts exceed 0.5%, demolition and reconstruction often become more cost-effective due to extensive damage to non-replaceable elements [1]. Furthermore, the economic impact is intensified by repair costs for structural and non-structural components, as well as business interruptions, which mutually challenge the seismic resilience of communities [2]. Consequently, there is a growing focus on developing innovative solutions to isolate and repair structural damage after seismic events. In this context, rocking systems have received increased attention and are regarded as effective seismic force-resisting systems for buildings designed to be more resilient [3]. Their capacity to endure significant earthquakes while exhibiting minimal residual drifts and limited structural damage concentrated at the rocking base interface is a key factor in this assessment [4]. This ability ultimately benefits modern resilient cities by reducing the expenses related to service interruptions for structural repairs or replacements.

The rocking mechanism acts as an isolation strategy, which allows the structure to rock during earthquakes, significantly reducing accelerations and forces and consequently enhancing resilience against extreme earthquakes [5]. The rocking mechanism aims to minimize residual drifts and structural damage by softening the seismic response and permitting elastic gap opening (rocking base) instead of yielding the primary structural elements. The integration of unbonded post-tensioned (PT) steel bars, designed to remain elastic, into masonry walls provides a restoring force that enables self-centering behavior, allowing the wall to return to its vertical position with minimal residual drifts post-earthquake events. As a result, rocking walls exhibit nonlinear elastic behavior dominated by rocking deformations rather than traditional flexural or shear modes [6]. External energy dissipation (ED) devices are often included to further enhance ED and displacement control during seismic events while facilitating access for post-earthquake repairs or replacement.

Early research on rocking masonry walls primarily focused on using unbonded PT steel strands or bars to achieve two critical objectives: restoring the wall to its vertical position after uplift and providing strength and stiffness post-decompression [7-11]. During uplift, PT steel elongates, thus increasing stress and enhancing the wall's moment resistance. Kalliontzis et al. [12] introduced rubber pads beneath the toes of a full-scale masonry wall with unbonded PT, preventing masonry damage and reducing strength degradation at larger drifts. However, the use of PT steel presents challenges, including construction complexities, inspection difficulties, and potential loss of self-centering capability if the PT steel yields.

To address such challenges, Yassin et al. [13] introduced an alternative approach that excluded PT steel, relying instead on gravitational loads for self-centering. The proposed controlled rocking masonry walls (ED-CRMWs) are equipped with internal ED devices to control maximum displacements. The study further explored confining plates and boundary elements at wall ends to reduce the damage to toes, as recommended by earlier research [14-18]. ED-CRMWs demonstrated the ability to sustain large drifts (up to 5%) while maintaining residual drifts below 0.15%. However, Yassin et al. [13] noted that placing ED devices inside walls limited their accessibility for post-earthquake repairs.

Recent advancements have focused on externally mounted ED devices to address these repairability concerns. Studies by Li [19] and East et al. [20] introduced replaceable steel flexural arms as external ED

components. Experimental and numerical analyses confirmed the efficiency of these arms, with design equations developed to support their integration into ED-CRMW systems.

The current study builds upon these innovations by examining the lateral behavior of CRMWs that incorporate rubber pads under the wall toes to prevent masonry crushing, use gravity loads for self-centering, and feature steel flexural arms as ED devices to dissipate seismic energy and control lateral displacement. The study presents experimental results from snap-back and quasi-static tests, providing insights into the seismic performance, self-centering ability, and ED capacity of these walls.

EXPERIMENTAL PROGRAM

Wall Description

The experimental program investigated the performance of a one-story, fully-grouted, half-scale masonry wall constructed using half-scaled concrete masonry blocks. These blocks were accurate replicas of the full-scale 200 mm units commonly used in North America. Fig.1 illustrates the elevation and side views of the wall and its top masses. The wall measured 1330 mm in length, 2000 mm in height, and 90 mm in thickness, resulting in an aspect ratio of 1.5. To prevent toe crushing during rocking motions, reinforced rubber pads, each 200 mm in length and 12.7 mm in thickness, were installed beneath the corner masonry toes. Such pads have a Shore hardness of 90 and experience minimal creep deformation when subjected to long-term loads. They are also resistant to water, mildew, brine, and fluctuations in temperature.

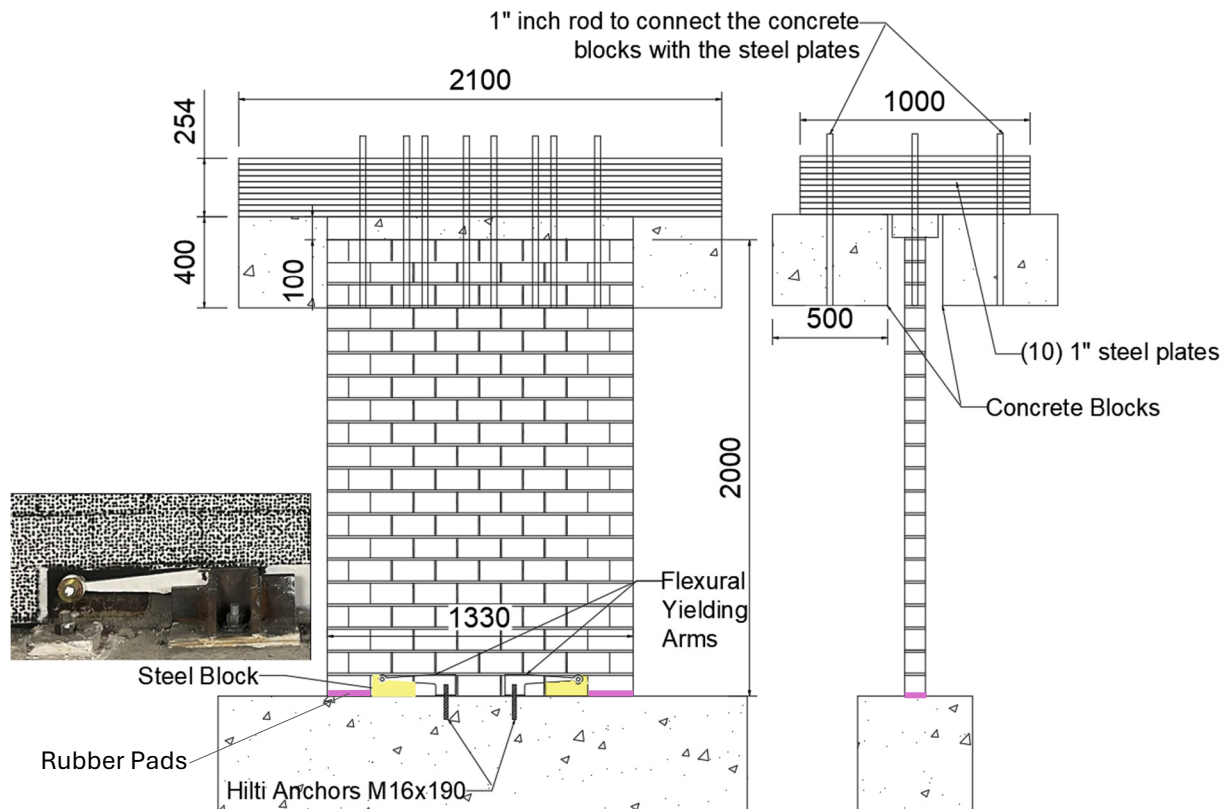


Figure 1: Geometrical details of the wall and top masses (dimensions in mm)

To facilitate the installation of the flexural arms, two custom hollow steel blocks were fabricated in the laboratory. These blocks matched the dimensions of the masonry units (90 mm x 90 mm x 185 mm) and

were constructed by welding steel plates. Their internal surfaces were roughened with grooves to improve bonding with the grout. The steel blocks were positioned in the second-to-last corner block on either side of the first course, allowing for secure connections to the wall's flexural arms.

A top mass of 8.5 tons was applied to the wall to replicate the mass as in seismic conditions. This mass was composed of ten steel plates (2100 mm x 1000 mm x 25.4 mm) and two reinforced concrete blocks (2100 mm x 500 mm x 400 mm). The mass provided axial compression equivalent to $3.8\% A_g f'_m$, where A_g is the cross-sectional area and f'_m is the masonry compressive strength. To distribute the load effectively, a reinforced concrete pad, 200 mm wide and 100 mm thick, was cast at the top of the wall, securing the attachment of the mass.

The wall included the minimum bonded vertical reinforcement required by CSA S304-24 [19] to meet seismic detailing standards. These reinforcement bars, with a cross-sectional area of 50 mm^2 (D7 bars), were terminated at the wall-foundation interface, ensuring that these bars did not contribute to the overall strength. The primary purpose of such bars was to maintain the wall's integrity during rocking motions. To transfer the force between the flexural arm and the masonry wall, M10 bars were welded to the steel block base. Fig.2 shows the cross-sectional view of the wall with its reinforcement layout and details.

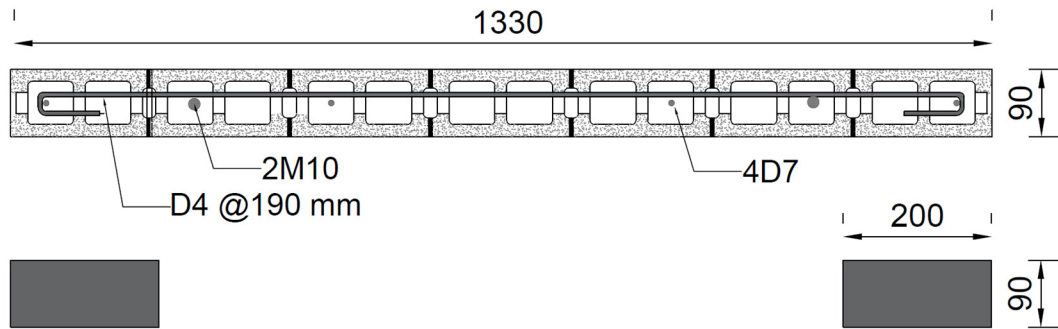


Figure 2: Cross-sectional view at midheight and rubber pads at the wall base (dimensions in mm)

Steel flexural yielding arms, serving as ED devices, were installed symmetrically, with two positioned on each side of the wall, as shown in Fig.3. Each arm measured 225 mm in length and 12.7 mm in thickness and was fabricated from Grade 44W steel using water jet cutting. The arms were anchored to the foundation with Hilti HDA M16x190 undercut anchors and connected to the wall via pins located 250 mm from the wall toes.

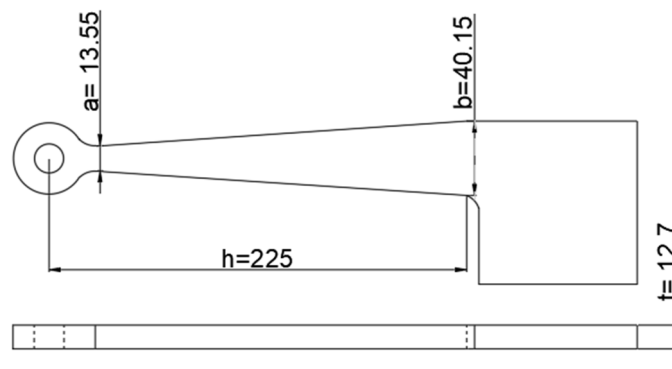


Figure 3: Configuration and dimensions of the flexural arms (dimensions in mm)

Wall Design

To determine the flexural strength of the wall, a sectional analysis was performed on the cross-section above the foundation, assuming a linear distribution of strain. The analysis applied a modified version of the equation provided by TMS [22] to calculate an equivalent stress block depth, denoted as a , incorporating the yield force F_y of the flexural arms, as presented in Eq.[1]. Additionally, the yield force F_y of the flexural arms was predicted using Eq.[2], developed by East et al. [20]. Finally, the wall's lateral strength was determined by dividing the nominal moment capacity M_n , calculated using Eq.[3], by the height of the wall.

$$(1) a = \frac{\sum_{i=1}^n F_{y_i} + P}{0.8f'_m t_w}$$

$$(2) F_y = \frac{4}{27} \frac{b^2 t \sigma_y}{h}$$

$$(3) M_n = \sum_{i=1}^n F_y \left(d_i - \frac{a}{2} \right) + P \frac{L_w - a}{2}$$

In the previous equations, P represents the total gravity load applied to the wall, f'_m is the masonry compressive strength, t_w is the wall thickness, b is the largest depth of the tapered flexural arm, t is the thickness of the flexural arm, σ_y is the yield stress of the steel arm, h is the length of the flexural arm, d_i is the distance from the wall toe to the flexural arm pin, and L_w is the wall length.

To ensure the self-centering behavior of the system, the ratio of the moment contributions from ED devices to those from restoring forces due to gravity loads must remain below 1. For this experimental study, the wall was designed with a ratio of 0.35, prioritizing self-centering capacity while maintaining adequate ED.

Wall Construction

The wall was constructed with half-scale mortar joints, 5 mm thick, replicating the 10 mm joints in full-scale masonry. Skilled masons built the wall using a running bond pattern with face-shell mortar bedding, following standard North American practices. Horizontal reinforcement was accommodated by saw-cutting 20 mm deep notches into the masonry unit webs. Rectangular rubber pads were positioned beneath the masonry toes to reduce stress concentrations in the toe region while maintaining lateral strength. A 12.5 mm thick mortar layer was applied along the wall-foundation interface to ensure full contact, except at the rubber pad locations.

The construction progressed in phases. The first six courses were built and grouted with high-slump grout containing 5 mm aggregate. This was followed by an additional six courses, grouted similarly, and then the final eight courses were built. Next, formwork was installed for the reinforced concrete (RC) pad, and eight threaded steel rods were embedded at the wall's top to secure the masses. Reinforcement for the pad was added before the final grouting.

Three four-blocks high by one-block long (375 mm high x 185 mm long x 90 mm thick) fully grouted masonry prisms were tested at each stage for compressive strength, yielding an average $f'_m = 18.2$ MPa. Tension tests on six steel coupons from the flexural arm plates showed a yield strength of 450 MPa and an ultimate strength of 510 MPa. To evaluate the compressive behavior of the rubber pads used in the wall system, cyclic compression tests were conducted on three cylindrical specimens with dimensions of 30 mm in diameter and 12.7 mm in thickness. The rubber pads exhibited a maximum compressive strength of 98.5 MPa at a strain of 38%.

The reinforced concrete footing was anchored to the strong floor at McMaster University's Applied Dynamics Laboratory. A mortar layer ensured proper levelling of the wall foundation. The wall was braced against out-of-plane movement at mid-height and the top masses with a roller support system. A steel

loading beam was welded to the top masses, with the embedded rods extending and welded to the beam for even load distribution.

Instrumentation Details

To monitor the vertical displacements occurring at various points on the wall, fifteen vertical linear potentiometers, labelled V1 through V15 were installed as shown in Fig.4. Specifically, three potentiometers (V1, V3, V5) were placed 50 mm above the wall-foundation interface to measure the gap openings at the base resulting from rocking motions. Each flexural arm had a vertical potentiometer attached to its pinned end, denoted as V2 and V4. The remaining ten vertical potentiometers (V6-V15) were distributed along the height of the wall to measure the relative vertical displacements between specific points.

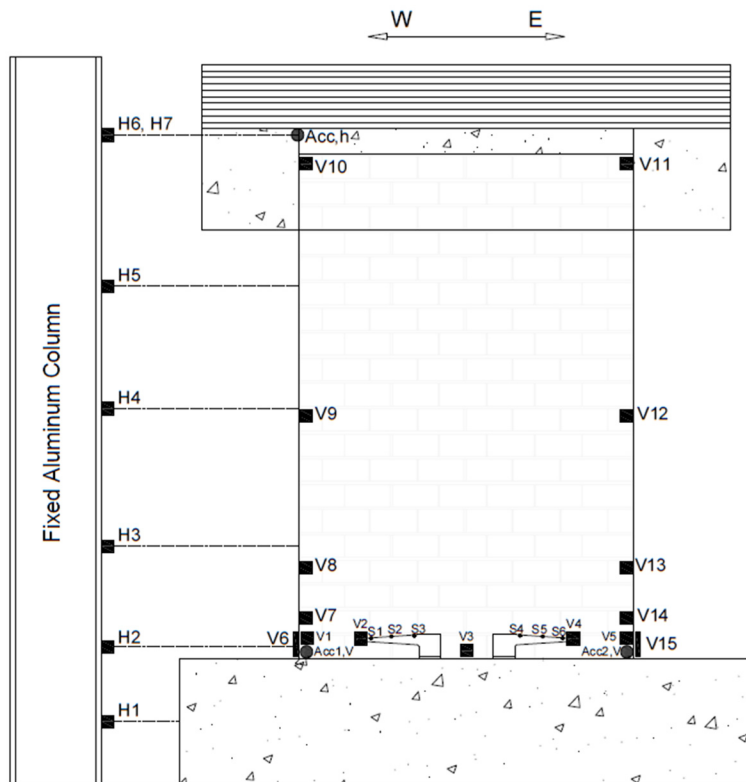


Figure 4: Instrumentation Layout

For lateral displacement measurements, five horizontally mounted linear potentiometers (H2-H6) were installed. Additionally, two horizontal potentiometers were used to detect any relative sliding: H1 monitored potential slip between the wall and the foundation at the base, while H7 measured sliding between the wall and the masses placed atop it. To record dynamic responses during testing, two vertical accelerometers at the rocking toes of the wall and a horizontal accelerometer at the top were installed.

Strain gauges were used to observe and record the progression of yielding within the ED devices. Specifically, six strain gauges (S1-S6) were attached to the upper and lower surfaces of each flexural arm to measure strains resulting from flexural deformations. An additional seven strain gauges (S7-S13) were installed on the outermost vertical reinforcement bars and the horizontal reinforcement within the wall to monitor strain developments in the reinforcing steel.

Loading Protocol

To evaluate the wall's capacity for ED through dynamic and hysteretic effects, as well as its response to lateral loading, a series of snap-back tests was conducted followed by quasi-static cyclic testing. Table 1 outlines the target initial conditions for all snap-back tests performed during the study. In these tests, lateral forces or displacements were applied to the wall using an MTS hydraulic actuator with a load capacity of 500 kN. Each snap-back test involved loading the wall to a predetermined lateral force or displacement. Once the target was reached, the actuator was disengaged rapidly using a quick-release mechanism, allowing the wall to enter free vibration. This allowed the dynamic response of the wall, including potential impact effects during rocking, to be examined in a more repeatable and systematic manner than would be possible with shake table testing. The maximum displacement during snap-back testing was limited to 2.0% drift, following the loading protocol followed by Kalliontzis et al. [12]. This drift ratio also aligns with the DS3 (Severe Damage) identification criterion for conventional reinforced masonry shear walls according to FEMA P58 [23].

Table 1: Target initial conditions for the snap-back tests

Test Sequence	Initial Top Lateral Drift or Peak Lateral Loads	Control Mode
1,2	7.5 kN	Load
3,4	15 kN	Load
5,6	22.5 kN	Load
7,8	2 mm (0.1%)	Displacement
9,10	4 mm (0.2%)	Displacement
11,12	7 mm (0.35%)	Displacement
13,14	10 mm (0.5%)	Displacement
15,16	15 mm (0.75%)	Displacement
17,18	20 mm (1.00%)	Displacement
19,20	25 mm (1.25%)	Displacement
21,22	30 mm (1.5%)	Displacement
23,24	35 mm (1.75%)	Displacement
25,26	40 mm (2.00%)	Displacement

Following the completion of all the snap-back tests, the flexural arms were replaced to ensure consistent test conditions. The wall was then subjected to quasi-static cyclic loading according to FEMA 461 [24] protocol. This loading protocol specifies that each displacement cycle is repeated twice, with the amplitude of each subsequent cycle increasing by 40% compared to the previous one. The quasi-static testing progressed until a drift of 5% was reached. Testing was concluded at the 5% lateral drift to prevent the top masses from contacting the out-of-plane roller plates at the top of the wall.

EXPERIMENTAL RESULTS

During the snap-back and quasi-static tests, the wall responded to lateral loads predominantly by rocking characterized by a gap opening at the wall base rather than bending along its height. No signs of shear or flexural cracks were observed during the test, as the dominance of rocking behaviour reduces the damage to the wall panel itself. At drift ratios starting from 0.08%, a gap began to form at the base rocking interface of the wall as the rocking motion started. As the lateral drift increased further, the flexural arms began to yield, initiating ED for the wall. The wall reached its design lateral strength at a drift ratio of 1.25%. As noted by East et al. [20], the flexural arms did not demonstrate a distinct yield plateau since they were designed to yield gradually throughout their entire cross-section and length. As a result, the stiffness of the

walls varied continuously. Due to the connection between the flexural arms and the wall foundation, there was no sliding between the wall and the foundation throughout the entire test.

The self-centering capability of the wall was evaluated by measuring the lateral drift at the point where the lateral force returned to zero after each pull-back test. Fig.5 shows the relationship between the residual drift observed and the initial drift applied in each test. Throughout all snap-back tests, the wall consistently exhibited residual drifts of less than 0.03%. These drifts are significantly below the 0.2% residual drift threshold specified for damage state DS1 (no structural realignment is necessary for structural stability) in Table C-1 of FEMA P58 [23], indicating that the wall maintained its structural integrity without the need for any repairs or realignment.

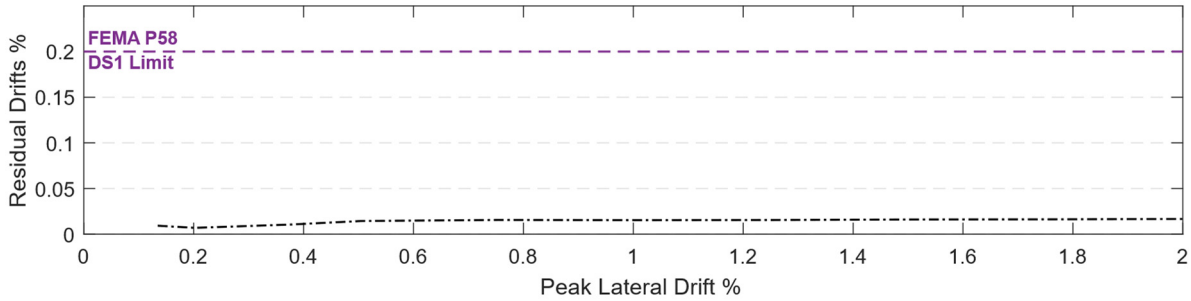


Figure 5: Residual drifts after snap-back testing

To calculate the total equivalent viscous damping ratio (ξ) for free vibration motions, the logarithmic decrement method was employed, as expressed in Eq.[4]:

$$(4) \xi = \ln \left[\frac{d_{i+1}}{d_i} \right]$$

In this equation, d_i and d_{i+1} represent the drifts at two consecutive positive or negative peaks, denoted as i and $i+1$, respectively. As shown in Fig.6, the damping ratio ξ exhibited varying values depending on the drift levels during the wall's motion. The values of ξ were around 3.5% for lateral drifts between 0.4% and 1.2%, with values reaching 7.5% at drifts lower than 0.1%. These high damping values at lower displacements are attributed to the wall engaging more of its elastic stiffness, which enhances ED through internal material damping and interactions with the rubber pads. The stiffer response limits motion, causing the system to dissipate more energy relative to the motion amplitude. Additionally, the damping ratio increased at drift ratios higher than 1.6%, reaching 6% at 2% lateral drift. This rise in EVD value is due to ED by the strain hardening of the flexural arms in addition to the energy absorption of the rubber pads.

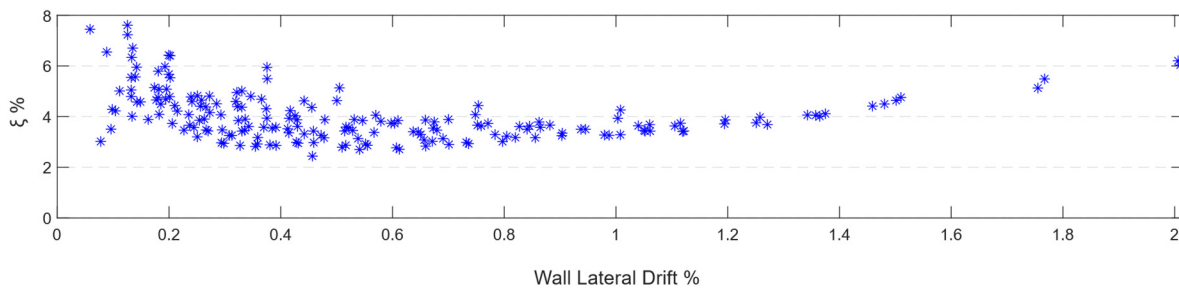


Figure 6: Equivalent viscous damping ratio

The force-drift response of the wall during the quasi-static test is presented in Fig.7. The wall shows maximum lateral strength values of approximately ± 32 kN and drift capacity exceeding $\pm 5\%$. These strengths are within 10% of the predicted wall strength of 35 kN, calculated using Equations (1-3). No strength degradation was observed throughout the test, and the wall maintained its structural integrity until the end of the test at 5% drift. The stable hysteretic behavior demonstrates effective ED through the yielding of flexural arms while maintaining reliable self-centering capabilities provided by gravity loads. The system achieved significant drift capacity without damage to the wall panel, with deformations primarily concentrated in the mortar layer underneath the wall in addition to compressive deformation in the rubber pads at drift levels above 3.5%, which is almost three times the design drift level. The consistent loops throughout the test indicate stable performance and excellent damage control strategy. By the end of the test, as shown in Fig.8, the masonry blocks at the toes remained undamaged, with significant damage observed primarily in the rubber pads at drifts exceeding 3.5% and the crushing of mortar beneath the wall at the rocking interface. The residual drifts were below the 0.2% residual drift threshold until 2% drifts. However, the residual drift values jumped to 0.65% in the final cycle at 5% drift, as shown in Fig.9, which could be explained by the damage observed in the rubber pads and accumulation of crushed mortar debris at the wall base which may cause unbalanced positioning of the wall with respect to the rocking interface. As the wall returns to its original position, this debris potentially interferes with complete gap closure, creating an offset in the measured displacements. Even so, the residual drifts remained below the DS3 threshold of 1% residual drift, indicating satisfactory self-centering capability even with pad damage at extreme drifts. The overall response demonstrates the successful implementation of a damage-resistant rocking system that effectively combines ED with self-centering capability.

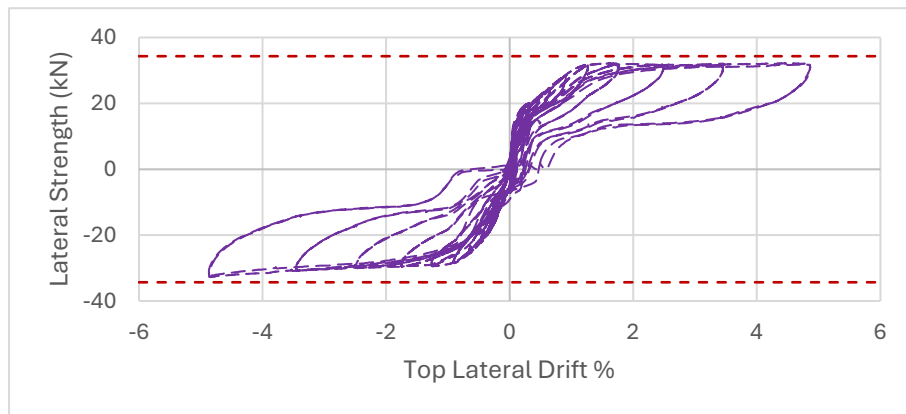


Figure 7: Hysteresis loops for the test wall

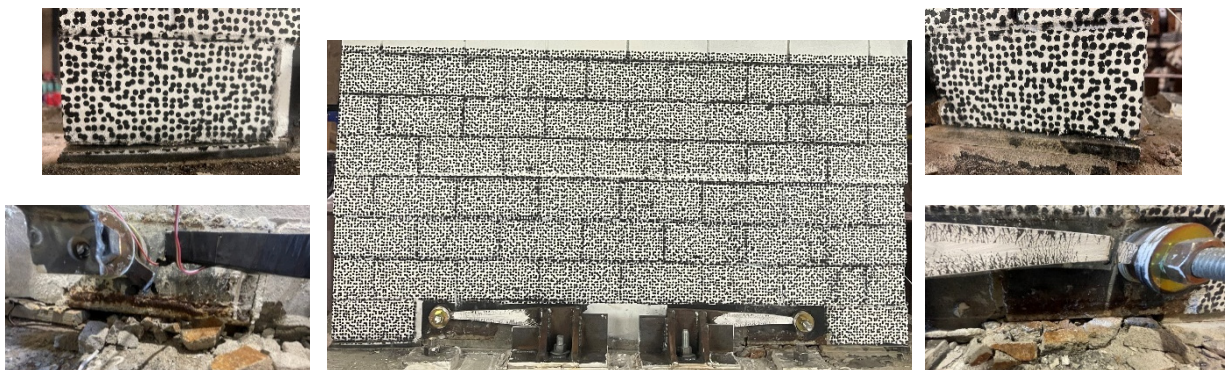


Figure 8: Test wall at the end of the quasi-static testing

The residual drifts measured during the snap-back tests were consistently lower than during the quasi-static test, as the wall exhibited a maximum residual drift of 0.2% up to 2% drift during the quasi-static testing, compared to 0.02% at the same drift in the snap-back testing. This indicates the system's tendency to self-center during the free vibration phase following ground motion, consistent with the findings of Henry et al. [25].

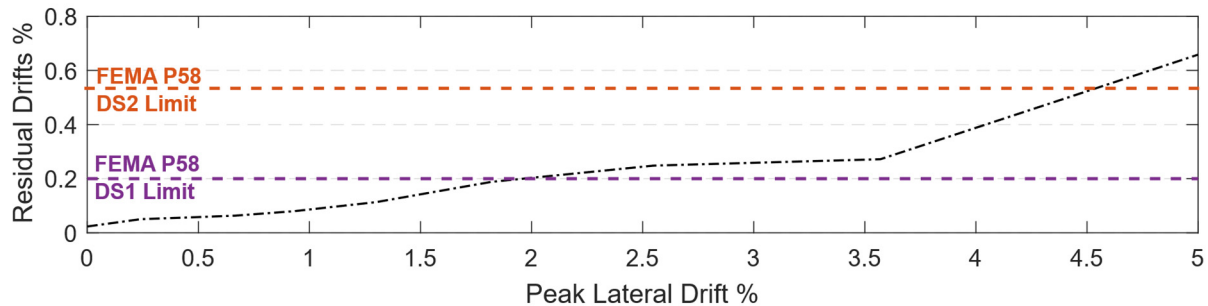


Figure 9: Residual drifts during quasi-static testing

CONCLUSION

This study presented an experimental investigation of a half-scale, fully grouted controlled rocking masonry wall featuring rubber pads under the wall's toes and equipped with flexural arms as ED devices. The rubber pads effectively protected the masonry blocks from damage at high lateral drifts, enhancing the wall's seismic performance. The wall exhibited excellent self-centering behavior, with residual drifts on the order of 0.02% following snap-back tests to drifts of 2%. It withstood lateral drifts up to 5% without any signs of strength degradation or damage to the masonry blocks above the rubber pads. The combination of gravity loads and supplementary ED devices maintained high-performance levels in terms of self-centering capability, minimal structural damage, and significant drift capacity. The proposed analytical equations accurately predicted the wall's strength within 10% of the experimental results. These findings demonstrate the effectiveness of incorporating rubber pads in controlled rocking masonry walls to enhance seismic performance, offering a promising solution for earthquake-resistant masonry construction. Future work could study the economic considerations of such a system, including both initial costs and long-term savings in post-earthquake repairs.

ACKNOWLEDGEMENTS

The financial support for this project was provided through the Canadian Concrete Masonry Producers Association (CCMPA), the Canada Masonry Design Centre (CMDCC), the Natural Sciences and Engineering Research Council (NSERC) and the Ontario Centres of Excellence (OCE).

REFERENCES

- [1] Erochko, J., Christopoulos, C., Tremblay, R. and Choi, H. (2011). "Residual Drift Response of SMRFs and BRB Frames in Steel Buildings Designed according to ASCE 7-05." *Journal of Structural Engineering*, 137(5), pp.589–599.
- [2] Ramirez, C.M. and Miranda, E. (2012). "Significance of residual drifts in building earthquake loss estimation." *Earthquake Engineering & Structural Dynamics*, 41(11), pp. 1477–1493.
- [3] Priestley, M. J. N., Sritharan, S., Conley, J. R., and Pampanin, S. (1999). "Preliminary results and conclusions from the PRESSS five-story precast concrete test building." *PCI Journal*, 44(6), 42-67.

- [4] Kurama, Y., Pessiki, S., Sause, R., and Lu, L.W. (1999). "Seismic behavior and design of unbonded post-tensioned precast concrete walls." *PCI Journal*, 44(3), 72-89.
- [5] Beck, J. L., and Skinner, R. I. (1974). "Seismic Response of a Reinforced Concrete Bridge Pier Designed to Step." *Earthquake Engineering & Structural Dynamics*, 2(4), 343-358.
- [6] Kalliontzis, D. and Schultz, A.E. (2017). "Improved estimation of the reverse-cyclic behavior of fully-grouted masonry shear walls with unbonded post-tensioning." *Engineering Structures*, 145, pp.83–96.
- [7] Laursen, P. T. and Ingham, J. M. (2001). "Structural Testing of Single-Story Post-Tensioned Concrete Masonry Walls." *The Professional Journal of The Masonry Society*, 19(1), 69-82.
- [8] Laursen, P. T. and Ingham, J. M. (2004a). "Structural testing of enhanced post-tensioned concrete masonry walls." *ACI Journal*, 101(6), 852-862.
- [9] Laursen, P. T. and Ingham, J. M. (2004b). "Structural testing of large-scale posttensioned concrete masonry walls." *Journal of Structural Engineering*, 130(10), 1497-1505.
- [10] Rosenboom, O. A., and Kowalsky, M. J. (2004). "Reversed in-plane cyclic behavior of posttensioned clay brick masonry walls." *Journal of Structural Engineering*, 130 (5), 787–798.
- [11] Hassanli, R., ElGawady, M., and Mills, J. (2016). "Experimental investigation of in-plane cyclic response of unbonded-posttensioned masonry walls." *Journal of Structural Engineering*, 142(5): 04015171.
- [12] Kalliontzis, D., Schultz, A.E. and Sritharan, S. (2022). "Unbonded post-tensioned structural masonry wall with rubber interface for limited-damage systems." *Journal of Structural Engineering*, 148(1): 04021223.
- [13] Yassin, A., Ezzeldin, M. and Wiebe, L. (2022). "Experimental Assessment of Controlled Rocking Masonry Shear Walls without Post-tensioning." *Journal of Structural Engineering*, 148(4), pp. 1-14.
- [14] Laursen, P.T. and Ingham, J.M. (2004). "Structural Testing of Large-Scale Posttensioned Concrete Masonry Walls." *Journal of Structural Engineering*, 130(10), pp.1497–1505.
- [15] Shedid, M.T., El-Dakhakhni, W.W. and Drysdale, R.G. (2009). "Behavior of fully grouted reinforced concrete masonry shear walls failing in flexure: Analysis." *Engineering Structures*, 31(9), pp.2032–2044.
- [16] Shedid, M.T., El-Dakhakhni, W.W. and Drysdale, R.G. (2011). "Seismic Response Modification Factors for Reinforced Masonry Structural Walls." *Journal of Performance of Constructed Facilities*, 25(2), pp.74–86.
- [17] Banting, B.R. and El-Dakhakhni, W.W. (2014). "Seismic Performance Quantification of Reinforced Masonry Structural Walls with Boundary Elements." *Journal of Structural Engineering*, 140(5): 04014001.
- [18] Ezzeldin, M., El-Dakhakhni, W. and Wiebe, L. (2017). "Experimental Assessment of the System-Level Seismic Performance of an Asymmetrical Reinforced Concrete Block–Wall Building with Boundary Elements." *Journal of Structural Engineering*, 143(8), 04017063.
- [19] Li, J. (2019). *Development of a Flexural Yielding Energy Dissipation Device for Controlled Rocking Masonry Walls*. MSc Thesis. McMaster University.
- [20] East, M., Li, J., Ezzeldin, M. and Wiebe, L. (2023). "Development of a Flexural Yielding Energy Dissipation Device for Controlled Rocking Systems." *Journal of Structural Engineering*, 149(1): 04022229
- [21] Canadian Standards Association and CSA Group (2024). *Design of masonry structures*. Mississauga, Ontario: CSA Group.
- [22] TMS (The Masonry Society) (2016). *Building Code Requirements and Specification for Masonry Structures*. TMS 402/602-16, Longmont, CO.
- [23] FEMA: *Seismic performance assessment of building*, FEMA-P58, Washington, DC (2018).
- [24] FEMA: *Interim testing protocols for determining the seismic performance characteristics of structural and nonstructural components*. FEMA 461, Washington, DC (2007).
- [25] Henry, R.S., S. Sritharan, and J.M. Ingham. (2011). "Recentering requirements for the seismic design of self-centering systems." *Proceedings of the Ninth Pacific Conference on Earthquake Engineering*, Auckland, New Zealand.